Graphene-Covered Photonic Structures for Optical Chemical Sensing

Borislav Vasić* and Radoš Gajić

Center for Solid State Physics and New Materials, Institute of Physics, University of Belgrade, Pregrevica 118, 11080 Belgrade, Serbia

(Received 27 March 2015; revised manuscript received 15 June 2015; published 11 August 2015)

Graphene applications in chemical sensing are based on the chemical doping of graphene. In this process, molecules adsorbed on graphene serve as charge-carrier donors or acceptors, thus changing the graphene conductivity. While the previous studies have been focused on chemical sensors with electrical detection, we theoretically investigate chemical sensing based on photonic structures covered with graphene. By considering chemical doping of graphene as a small perturbation, we show that optimal photonic structures operate at low-terahertz frequencies, with the reflectance intensity as the output signal. In order to achieve an efficient chemical sensing, photonic structures should provide the electric-field enhancement within the graphene plane. As a result, the proposed structure consists of the metallic mirror and quarter-wavelength-thick dielectric spacer with graphene on the top of it. The sensitivity is maximized when the Fermi energy in the graphene not exposed to the environment is around 30 meV. By taking the resolution for the reflectance measurement of 1%, we show that the proposed sensing structure can detect graphene doping by 150 electrons or holes per square micrometer in the dynamic range of around 3000 charge carriers.

DOI: 10.1103/PhysRevApplied.4.024007

I. INTRODUCTION

Most of the potential graphene applications in electronics and photonics are based on its tunable conductivity. It can be controlled electrically and chemically. In the first approach, charge carriers in graphene are induced by the electric-field effect [1]. In the chemical doping of graphene, adsorbed molecules serve as charge-carrier donors or acceptors, thus changing graphene conductivity [2–5]. Therefore, the chemical doping of graphene can be used for very efficient sensing of the adsorbed molecules [2]. High sensitivity of graphene stems from its two-dimensional nature and an extremely high surface-to-volume ratio, so even a small number of electrons can produce a significant change in graphene conductivity [2]. This graphene property was used to design very efficient gas [2,6–9] and biosensors [10–13], but only with electrical detection.

On the other hand, sensors with optical detection have several important advantages: larger sensitivity, selectivity, insensitivity on the electromagnetic interference, the possibility of multiplexing, faster operation, and electrical passiveness. Graphene applications in optical sensors were based on several mechanisms. Graphene was mostly used as a coating for plasmonic [14,15] and dielectric [16] sensors in order to increase the adsorption of molecules or to protect plasmonic films against oxidation [17–19]. Graphene oxide can fluoresce, so it was used as a quencher [20] or donor [21] in fluorescence-resonance energy-transfer sensors. Graphene microstructures supporting localized surface plasmons at midinfrared frequencies were used for sensing of the dielectric environment [22–25] and vibrational modes of thin molecular films [22,26–28]. Polarization-dependent absorption in graphene was applied for efficient refractive-index sensors as well [29].

Chemical doping of graphene embedded into optical sensors could enable the design of new optical chemical sensors [30–33] and further boost their sensitivity. Initial proposals for such sensors are given in Refs. [34,35]. Research on this topic has been started recently when this sensing mechanism has been investigated in optical fibers covered with graphene [36–39]. However, research in this field is still at the very beginning.

To tackle this problem, we investigate the efficiency of optical methods for the sensing of chemically doped graphene and consider the following issues: (1) an optimal detection method, that is, the choice between the wavelength interrogation and the intensity measurement; (2) geometry of an optical structure covered with graphene which can serve as a simple and efficient chemical sensor; (3) an optimal frequency range where the selected structure should operate; (4) an optimal graphene conductivity at the working point; and (5) sensitivity, dynamic range, and resolution of the graphene-based optical sensors. This paper presents an optimal sensing structure consisting of the metallic ground plane, a quarter-wavelength-thick dielectric spacer and graphene on the top. It operates at low-terahertz (THz) frequencies while the reflectance is taken as the output signal. Fermi energy of the graphene not exposed to the environment is kept at around 30 meV. As a

*bvasic@ipb.ac.rs

result, the proposed structure enables sensing of the graphene doping by around 150 electrons or holes per square micrometer.

II. SENSITIVITY OF GRAPHENE-BASED CHEMICAL SENSORS

The sensitivity of a graphene-based chemical sensor is the ratio between its output ΔY and a change in the concentration ΔN of molecules adsorbed on graphene:

$$S = \frac{\Delta Y}{\Delta N}. \tag{1}$$

When the molecule concentration is changed by ΔN, the concentration of charge carriers in graphene is changed by $\Delta N_g = \alpha_g \Delta N$, where $0 < \alpha_g < 1$. This means that every adsorbed molecule supplies graphene with α_g charge carriers. Therefore, the sensitivity S depends on the efficiency of the chemical doping and the specific type of the molecule adsorbed on graphene. For this reason, we consider the following sensitivity:

$$S_g = \frac{\Delta Y}{\Delta N_g}, \tag{2}$$

which depends only on the properties of graphene and selected sensor geometry. Sensing can be then divided into two processes: (1) the change in the graphene Fermi energy E_F due to the change in the charge-carrier concentration in graphene and (2) the change in the sensor output due to the change of Fermi energy. Sensitivities of these processes are S_{E_F} and S_Y, respectively, so then the sensitivity from Eq. (2) can be written as

$$S_g = S_{E_F} S_Y = \frac{\Delta E_F}{\Delta N_g} \frac{\Delta Y}{\Delta E_F}. \tag{3}$$

S_Y is determined by the selected sensor, while S_{E_F} depends only on graphene properties.

Electron and hole density in graphene are symmetric, so both densities depend on the graphene Fermi energy in the following way [40]:

$$N_g = \frac{2}{\pi}\left(\frac{k_B T}{\hbar v_F}\right)^2 F_1(\eta), \tag{4}$$

where N_g is the charge-carrier concentration in graphene, $F_j(\eta) = 1/\Gamma(j+1)\int_0^\infty du u^j/(1+e^{u-\eta})$ is the Fermi-Dirac integral of order j, $\eta = E_F/(k_B T)$, $u = E/(k_B T)$, E is the energy of charge carriers, k_B is the Boltzmann constant, T is a temperature, $v_F \approx 1.1 \times 10^6$ m/s is the Fermi velocity in graphene, and Γ is the gamma function. For $\eta \gg 1$, Eq. (4) becomes

$$N_g = \frac{E_F^2}{\pi \hbar^2 v_F^2}. \tag{5}$$

Then, S_{E_F} is given by the following approximation:

$$S_{E_F} = \frac{\pi \hbar^2 v_F^2}{2E_F}. \tag{6}$$

N_g calculated using Eq. (4) [41] and the approximation given by Eq. (5) is plotted in Fig. 1(a) as a function of E_F. The figure shows quite good overall matching between these two curves. However, the relative error between them is even 100% for low Fermi energy as shown in the right inset. This huge error is due to zero charge-carrier density given by the approximative formula for $E_F = 0$. On the other hand, the exact solution gives the finite value of $N_g = (\pi/6)[k_B T/(\hbar v_F)]^2$ [40], as shown in the left inset.

Sensitivity S_{E_F} is depicted in Fig. 1(b). The exact calculations are done by the numerical differentiation of Eq. (4). The minimal $E_F = 1$ meV is taken for better visibility. S_{E_F} continuously falls down with increasing E_F. The approximative formula is applicable only for E_F higher than 20–30 meV.

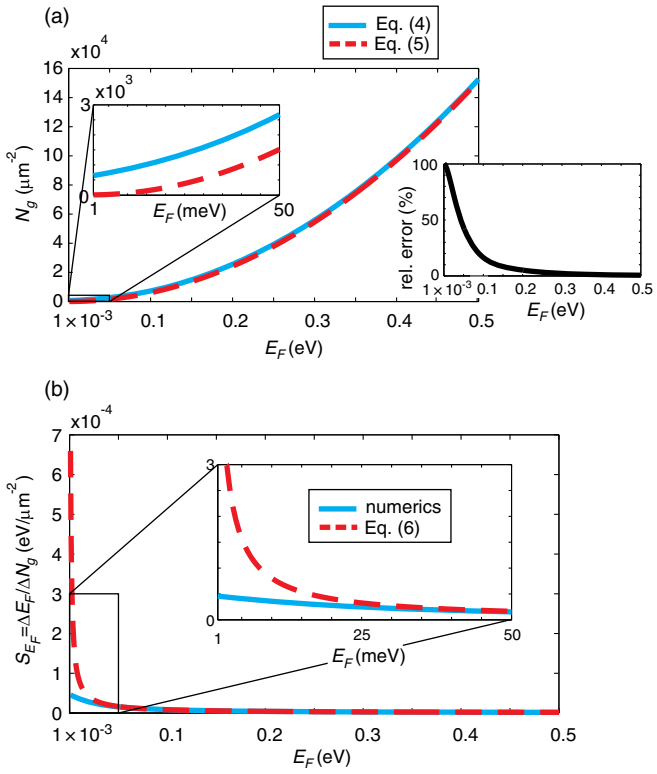

FIG. 1. (a) Charge-carrier concentration N_g as a function of Fermi energy E_F. The right inset shows the relative error between N_g calculated using Eqs. (4) and (5). (b) Sensitivity $S_{E_F} = \Delta E_F/\Delta N_g$ obtained by the numerical differentiation of Eq. (4) and approximative formula given by Eq. (6).

III. CHEMICAL DOPING OF GRAPHENE AS A PERTURBATION OF PHOTONIC STRUCTURES

We consider a general case where a photonic structure is coupled with a graphene. ω_1 is the eigenfrequency of the photonic structure with graphene whose conductivity and Fermi energy are $\sigma_{g,1}(\omega)$ and $E_{F,1}$, respectively. If the graphene is exposed to the environment, the chemical doping from adsorbed molecules changes the Fermi energy and conductivity to $E_{F,2}$ and $\sigma_{g,2}(\omega)$, respectively. At the same time, the eigenfrequency of the structure becomes ω_2. The change of the Fermi energy and the graphene conductivity due to the chemical doping are denoted as $\Delta E_F = E_{F,2} - E_{F,1}$ and $\Delta\sigma_g(\omega) = \sigma_{g,2}(\omega) - \sigma_{g,1}(\omega)$, respectively. ΔE_F is typically on the order of a millielectronvolt, so it can be regarded as a small perturbation of the system not exposed to the environment. According to the perturbation theory [42], a change of the eigenfrequency $\Delta\omega = \omega_2 - \omega_1$ is given by

$$\Delta\omega = -i\sigma_{g,1}(\omega)\frac{\int_S |\mathbf{E}_{xy,1}|^2 dS}{W_1}, \tag{7}$$

where S denotes graphene area, $\mathbf{E}_{xy,1}$ and W_1 are the electric field in the graphene plane, and the stored electromagnetic energy in the structure not exposed to the environment, respectively. According to Eq. (7), the change of the lifetime of the mode $\mathrm{Im}(\Delta\omega)$ is

$$\mathrm{Im}(\Delta\omega) = -\mathrm{Re}[\sigma_{g,1}(\omega)]\frac{\int_S |\mathbf{E}_{xy,1}|^2 dS}{W_1}, \tag{8}$$

while the spectral shift of the mode $\mathrm{Re}(\Delta\omega)$ is

$$\mathrm{Re}(\Delta\omega) = \mathrm{Im}[\sigma_{g,1}(\omega)]\frac{\int_S |\mathbf{E}_{xy,1}|^2 dS}{W_1}, \tag{9}$$

where Re and Im stand for the real and imaginary part of a complex value, respectively.

Graphene surface conductivity $\sigma_g(\omega)$ is calculated as a sum of the intraband σ_{intra} and interband term σ_{inter} [43]

$$\sigma_{\mathrm{intra}}(\omega) = i\frac{e^2 k_B T}{\pi\hbar^2(\omega + i\Gamma)}\left(\frac{E_F}{k_B T} + 2\ln(e^{-(E_F/k_B T)} + 1)\right), \tag{10}$$

$$\sigma_{\mathrm{inter}}(\omega) = i\frac{e^2}{4\pi\hbar}\ln\left(\frac{2E_F - (\omega + i\Gamma)\hbar}{2E_F + (\omega + i\Gamma)\hbar}\right), \tag{11}$$

where ω is the angular frequency, e is the elementary charge, $\hbar = h/2\pi$ is the reduced Planck's constant, $\Gamma = 10$ meV is the carrier scattering rate, and $T = 300$ K is the temperature. Graphene is modeled as a thin dielectric layer with the permittivity

$$\varepsilon_g = 1 + i\sigma_g/(\omega\varepsilon_0 t_g), \tag{12}$$

where $t_g = 0.34$ nm is the graphene thickness and ε_0 is the vacuum permittivity. In the following, only planar optical structures and normal incidence (the electric field is parallel to graphene) are considered, so the modeling of graphene with an isotropic permittivity is valid. Recently, it has been shown that the nonlocal effects, that is, the spatial dispersion, can affect graphene conductivity at low-terahertz frequencies [44]. The influence of the nonlocal effects becomes important in graphene nanostructures supporting propagating surface modes. This influence grows with q/k_0, where q is the radial wave number of the mode propagating along the graphene plane, whereas k_0 is the free-space wave number. However, in the following we will consider photonic resonators covered with a homogeneous graphene sheet which does not support propagating modes. Therefore, these resonators work at $q = 0$, where the nonlocal effects do not influence the graphene conductivity [44].

According to Eqs. (8) and (9), the chemical doping of graphene leads to amplitude changes in reflection and transmission spectra or the spectral shifting of optical resonances, respectively. Apart from the term $\int_S |\mathbf{E}_{xy,1}|^2 dS/W_1$, which is the same for both $\mathrm{Im}(\Delta\omega)$ and $\mathrm{Re}(\Delta\omega)$, the amplitude changes are directly proportional to $\mathrm{Re}[\sigma_{g,1}(\omega)]$, while the spectral shifts are directly proportional to $\mathrm{Im}[\sigma_{g,1}(\omega)]$. The real and imaginary part of graphene conductivity as a function of frequency and $E_{F,1}$ are depicted in Figs. 2(a) and 2(b), respectively.

As can be seen, $\mathrm{Re}[\sigma_{g,1}(\omega)]$ is maximized at low-terahertz frequencies (from 0.1 to 1 THz). On the other hand, $\mathrm{Im}[\sigma_{g,1}(\omega)]$ has a maximum at higher terahertz frequencies (from 1 to 10 THz). However, at higher terahertz frequencies, $\mathrm{Re}[\sigma_{g,1}(\omega)]$ is significant as well, resulting in huge losses thus masking any spectral shift. In order to estimate the influence of the graphene losses on the spectral shifting, the ratio between the imaginary and real part of graphene conductivity is plotted in Fig. 2(c). The ratio is maximized at midinfrared frequencies, so this is the range with the efficient spectral shifting. This graphene property has been used for a design of spectrally tunable planar metamaterials at the midinfrared frequencies [42,45,46]. However, a significant ratio $\mathrm{Im}[\sigma_{g,1}(\omega)]/\mathrm{Re}[\sigma_{g,1}(\omega)]$ can be achieved only for $E_{F,1}$ higher than approximately 0.1 eV, which blocks the interband transitions in graphene and lowers the corresponding losses. This is highlighted in the inset of Fig. 2(c), which shows the cross section of the main graph for 40 THz. Therefore, at midinfrared frequencies sensing structures should operate at higher Fermi energies. However, S_{E_F} then falls down, so the overall sensitivity is low.

By comparing $\mathrm{Re}[\sigma_{g,1}(\omega)]$ at low-terahertz frequencies and $\mathrm{Im}[\sigma_{g,1}(\omega)]$ at midinfrared frequencies for the same $E_{F,1}$, it follows that the amplitude change of the mode is larger than the spectral one. This is illustrated in Fig. 2(d) which shows the absolute value of the typical ratio between

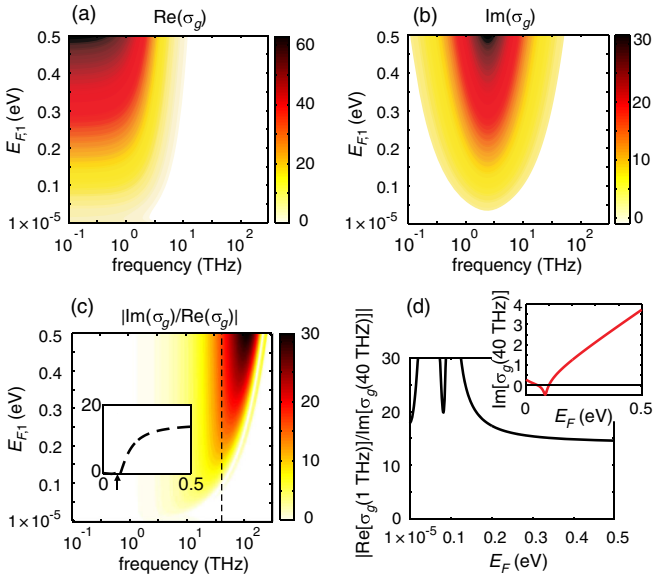

FIG. 2. Graphene conductivity as a function of frequency and Fermi energy: (a) The real part of σ_g. (b) The imaginary part of σ_g. (c) The absolute value of the ratio between the imaginary and real part of σ_g. The inset in part (c) shows the cross section for 40 THz [marked with a dashed vertical line in part (c)], while the arrow denotes the Fermi energy needed to block the interband transitions $E_F = \hbar\omega/2 = 82$ meV. (d) The absolute value of the ratio between the real part of σ_g at 1 THz and the imaginary part of σ_g at 40 THz, while the inset shows the imaginary part of σ_g at 40 THz.

the real part of σ_g at low-terahertz frequencies (here exactly at 1 THz) and the imaginary part of σ_g at midinfrared frequencies (here exactly at 40 THz). As can be seen, the real part of σ_g at low-terahertz frequencies is at least one order of magnitude larger than the imaginary part of σ_g at midinfrared frequencies. The ratio becomes infinite at $E_{F,1}$ around 0.1 eV due to zero $\mathrm{Im}(\sigma_g)$ [see the inset in Fig. 2(d)] so the curve in Fig. 2(d) is saturated for better visibility.

According to the previous analysis, two important outcomes follow: (1) The detection method of graphene-covered optical sensors should be based on intensity measurements, either reflection or transmission, rather than on wavelength interrogation (based on the spectral shifts of optical resonances). (2) Graphene-covered optical sensors should operate at low-terahertz frequencies.

IV. GEOMETRY OF PHOTONIC STRUCTURES FOR CHEMICAL SENSING

The next task is to find an optimal geometry of a photonic structure for chemical sensing. Even a free-standing graphene at low-terahertz frequencies would produce a significant change in reflectance and transmittance due to the chemical doping. For example, $\Delta E_F =$ 10 meV in the freestanding graphene produces around $a0.1\%$ change in the reflectance and transmittance at low-terahertz frequencies. However, this change is rather small. Therefore, it is necessary to couple graphene with a photonic structure in order to increase the magnitude of the electric field $\mathbf{E}_{xy,1}$ in the graphene plane and to increase the change of the mode lifetime in accordance to Eq. (8). The next reason for putting graphene on an appropriate substrate is to provide an easy way to control Fermi energy in graphene by a bias voltage in order to define a working point $E_{F,1}$. In addition, the photonic structure to be coupled with graphene should be simple in order to facilitate fabrication and realistic applications, and graphene should be exposed to the environment so molecules from a medium to be sensed can reach the graphene surface.

Selected geometry for the graphene-based chemical sensor is shown in Fig. 3. It consists of graphene lying on an electromagnetic resonator consisting of a dielectric spacer and bottom metallic mirror. The sensor is very simple and compatible with graphene since it consists of only planar layers. Fabrication would be feasible since similar structures have been experimentally realized and used as electro-optical modulators [47,48]. Normal incidence is considered, and the change in the reflected field is taken as a sensor output in a function of graphene doping. The dielectric spacer has a quarter-wavelength thickness so the refractive index n_d and thickness of the spacer t_d are related by the expression $n_d t_d = \lambda_0/4$, where λ_0 is the wavelength of the lowest resonance of the structure. Together with the metallic mirror, the spacer ensures that the maximal electric field of the resulting standing wave is exactly within the graphene plane. This will provide the most important requirement—the electric-field enhancement in the graphene plane. The metallic mirror also provides a back gate for graphene in order to adjust the Fermi level at the working point.

Large electric-field enhancement in graphene can be achieved in combination with other optical structures, such as plasmonic structures and metamaterials [42,45,46,49], photonic-crystal cavities [50,51], and Fabry-Perot cavities [52–54]. However, photonic structures producing larger electric-field enhancement do not necessarily give a greater change in the mode lifetime. Namely, $\mathrm{Im}(\Delta\omega)$ from Eq. (8) is determined by the electric field in the photonic structure with already-embedded graphene, not in the bare structure without graphene. When graphene is inserted, it always absorbs a part of an incident radiation, thus decreasing the magnitude of the electric field. If a photonic structure generates larger electric fields, graphene absorbs the incident radiation more efficiently. In the considered case, the absorption in graphene is very pronounced since sensing structures operate at low-terahertz frequencies where graphene is highly conductive.

The electric field in the proposed sensing structure is compared to the Fabry-Perot cavity depicted in Fig. 3(b). The Fabry-Perot cavity is formed by adding the Bragg mirror on the top of the structure from Fig. 3(a). Although the Fabry-Perot cavity is not appropriate for chemical

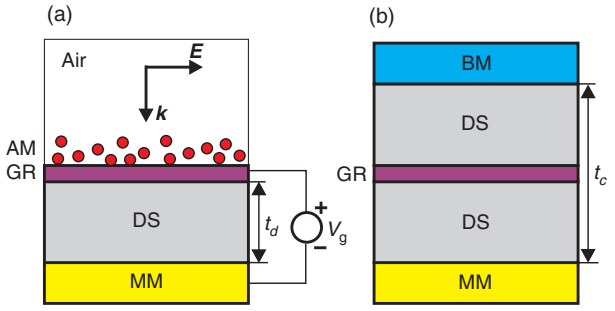

FIG. 3. (a) Proposed geometry for a graphene-based photonic device intended for chemical sensing and biosensing. (b) Corresponding Fabry-Perot cavity serving for the comparison of the electric-field enhancement. The Bragg mirror on the top of the cavity is formed from a $(HL)^3H$ multilayer structure, where H and L stand for the layers with high (2.23) and low (1.41) refractive index, respectively. MM stands for the metallic mirror, DS stands for the dielectric spacer, GR stands for graphene, AM stands for adsorbed molecules (schematically represented by dots) on graphene, and BM stands for the Bragg mirror.

sensing since graphene it is not exposed to the environment, it serves as a simple structure producing larger electric fields. All numerical calculations are done using the RETICOLO code based on the rigorous coupled-wave analysis [55]. Figure 4 shows the comparison of electric-field magnitudes produced in the proposed sensing structure and the corresponding Fabry-Perot cavity. Both resonators operate at 0.3 THz. As can be seen in Fig. 4, the Fabry-Perot cavity generates the standing wave with around 5 times larger magnitude than the proposed sensing

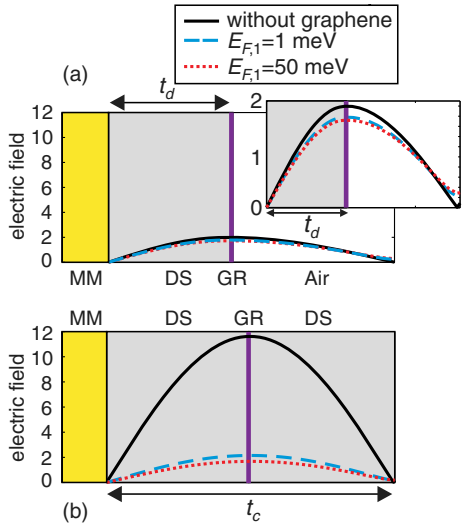

FIG. 4. Magnitude of the electric field at resonance for the structure from (a) Fig. 3(a) and (b) Fig. 3(b). In part (a), the inset shows the enlarged field distribution. For the structures with graphene, the electric-field magnitude is plotted for $E_{F,1} = 1$ meV and $E_{F,1} = 50$ meV. The graphene position is marked with the vertical line. MM stands for metallic mirror, DS stands for dielectric spacer, and GR stands for graphene.

structure in the case without graphene. However, when graphene is inserted, this ratio is around 1.5 for $E_{F,1} = 1$ meV and only 1.12 for $E_{F,1} = 50$ meV. The same would happen for other electromagnetic resonators with large electric-field enhancement without graphene (plasmonic structures, metamaterials, and photonic-crystal cavities). Therefore, they would not give a significantly larger electric field when graphene is inserted, while they are much more complex than the proposed structure.

V. SENSITIVITY OF GRAPHENE-COVERED TERAHERTZ RESONATORS

The sensor output for the chosen structure is reflectance $Y = R$. In order to calculate the second term from Eq. (3), the sensitivity $S_Y = S_R = \Delta R/\Delta E_F$, the photonic structure from Fig. 3(a) with the following parameters is considered: $n_d = 1.41$, $t_d = 177$ μm, whereas the lowest resonance is adjusted at $f_0 = 0.3$ THz. Since the device operates at low-terahertz frequencies, in all of the following calculations the interband conductivity is neglected so $\sigma_g(\omega) = \sigma_{\text{intra}}(\omega)$. The change of the refractive index above graphene due to adsorbed molecules is neglected, so the reflectance is changed only due to chemical doping. In a general case, the overall sensitivity would be enhanced by taking into account the refractive-index sensitivity.

Reflectance from this resonator as a function of frequency and Fermi energy $E_{F,1}$ is shown in Fig. 5(a). Dips in the reflectance around $f_0 = 0.3$ THz, $3f_0 = 0.9$ THz, and $5f_0 = 1.5$ THz denote the first, second, and third resonances of the structure. Cross sections of the map in Fig. 5(a) are shown in Fig. 5(b) for all three resonant frequencies.

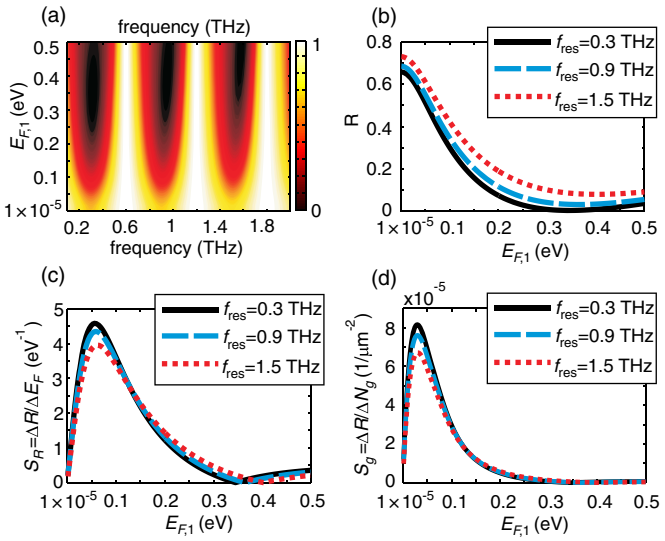

FIG. 5. (a) Reflectance map as a function of frequency and working point $E_{F,1}$. (b) Cross section of the map in part (a) for three specified resonant frequencies. (c) Sensitivities S_R obtained as derivatives of the curves from part (b). (d) Sensitivities S_g obtained from the numerical results in Figs. 1(b) and 5(c).

Sensitivities $S_R = \Delta R/\Delta E_F$ are obtained as derivatives of these curves and they are shown in Fig. 5(c). As can be seen, the maximal sensitivity is reached for $E_{F,1} \approx 60$ meV. According to Eq. (8), the change of the mode lifetime depends on $\mathrm{Re}[\sigma_{g,1}(\omega)]$ and the electric field in the graphene plane. According to Fig. 2(a), $\mathrm{Re}[\sigma_{g,1}(\omega)]$ grows with Fermi energy. On the other hand, the in-plane electric field in graphene falls with $E_{F,1}$ due to increased absorption in graphene as already shown in Fig. 4. Then there is an optimal $E_{F,1}$ which enables the maximal change of the reflectance for a small change in the Fermi energy. Operation at all three resonances gives similar sensitivities.

Sensitivity S_g from Eq. (2) is calculated by multiplying numerically obtained S_{E_F} [given in Fig. 1(b)] and S_R [given in Fig. 5(c)]. It is depicted in Fig. 5(d). S_g has a similar shape as the sensitivity S_R, while the maximum, now at around 30 meV, is shifted to lower $E_{F,1}$ due to the influence of S_{E_F}. In the calculations of the sensitivity S_g, it is of crucial importance to take numerically calculated S_{E_F}, since the approximative S_{E_F} given by Eq. (6), gives maximal S_g at zero $E_{F,1}$.

VI. SENSING MECHANISM

The sensing mechanism is illustrated in Fig. 6(a) for the structure with the spacer refractive index and thickness $n_d = 1.41$ and $t_d = 177$ μm, respectively, the lowest resonance $f_0 = 0.3$ THz. The solid line shows the reflectance spectrum for the structure with graphene and $E_{F,1} = 30$ meV corresponding to the case when the graphene is not exposed to the environment. The reflection dip in the spectrum corresponds to the resonance of the structure. An increase of Fermi energy by ΔE_F results in a lower reflectance. This amplitude change of the reflectance is maximized at the resonance and can be used for chemical sensing. Figure 6(b) shows the change of the reflectance at the lowest resonance $f_0 = 0.3$ THz as a function of ten discrete values of ΔE_F. At the same time, the corresponding ΔN_g is shown. It can be seen that the sensor has a linear response with the sensitivity $S_g = 8 \times 10^{-5}$ $1/\mu\mathrm{m}^{-2}$ (the slope of the curve connecting points obtained by the numerical calculations). This is a more than one order of magnitude higher sensitivity than the sensitivity of the corresponding resonator without a metallic mirror with $S_g = 5 \times 10^{-6}$ $1/\mu\mathrm{m}^{-2}$ [the results are shown in Fig. 6(b)]. Also, this is a $40\times$ larger sensitivity compared to the freestanding graphene which is analyzed at the beginning of Sec. IV.

In order to determine the dynamic range with the specified sensitivity, the reflectance as a function of ΔN_g is calculated for ΔE_F up to 120 meV. The results are shown in Fig. 7(a) for $E_{F,1} = 30$ meV. As can be seen, ΔR linearly depends on N_g in the range $\Delta N_g \approx 3 \times 10^3$ $\mu\mathrm{m}^{-2}$ [this area is denoted with a gray rectangle in Fig. 7(a)]. Here, ΔR is approximated with the linear dependence $S_g \Delta N_g$, where $S_g = 6.7 \times 10^{-5}$ $1/\mu\mathrm{m}^{-2}$.

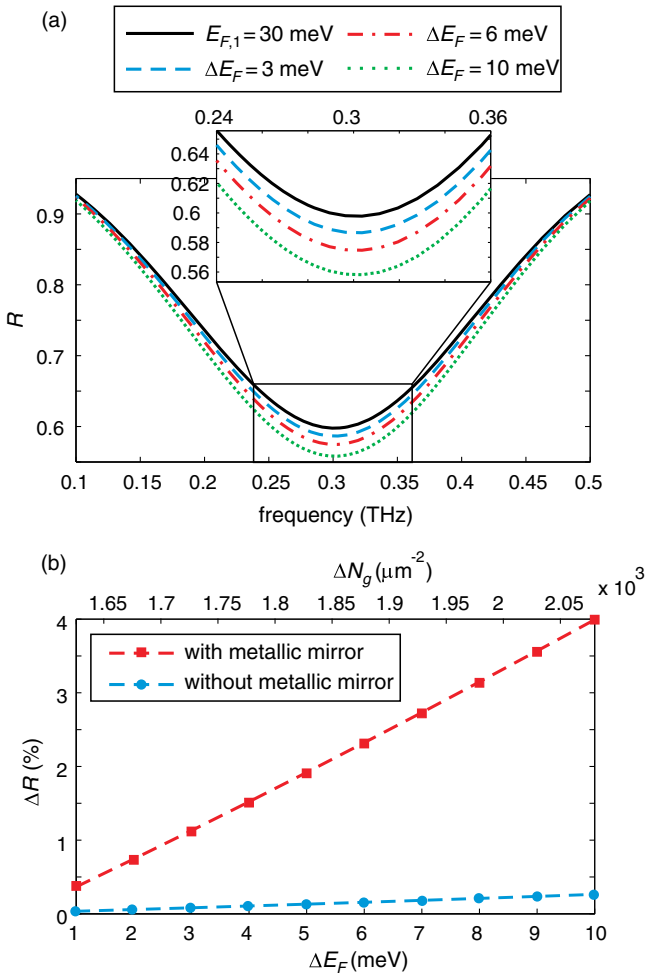

FIG. 6. (a) Reflectance as a function of frequency: $E_{F,1} = 30$ meV and three values of ΔE_F. (b) Change of the reflectance (in percents) as a function of the change in the Fermi energy. Reflectance for the resonator without metallic mirror is shown for comparison.

The sensor resolution is calculated as $\sigma = \sigma_{\mathrm{instr}}/S_g$, where σ_{instr} is the instrumental resolution [31]. σ_{instr} is determined by the noise level at the sensor output. In the considered case, it is the resolution of terahertz spectrometers for the reflection measurement. By taking a realistic value $\sigma_{\mathrm{instr}} = 0.01$ (this corresponds to the resolution of 1% for the reflection measurements) [56], the achieved resolution is $\sigma \sim 150$ $\mu\mathrm{m}^{-2}$. According to Ref. [2], this corresponds to the sensitivity of around 2 ppm. The proposed sensing structure operating at $E_{F,1} = 30$ meV can detect graphene doping in discrete steps, each of them corresponding to the doping with around 150 electrons or holes per square micrometer. In the dynamic range of $\Delta N_g \approx 3 \times 10^3$ $\mu\mathrm{m}^{-2}$, the structure can detect 20 such discrete events, each resulting with around 1% reflectance change, as depicted in Fig. 7(b).

The considered terahertz resonator enables multiband operation as can be seen from Fig. 5. The resonances are

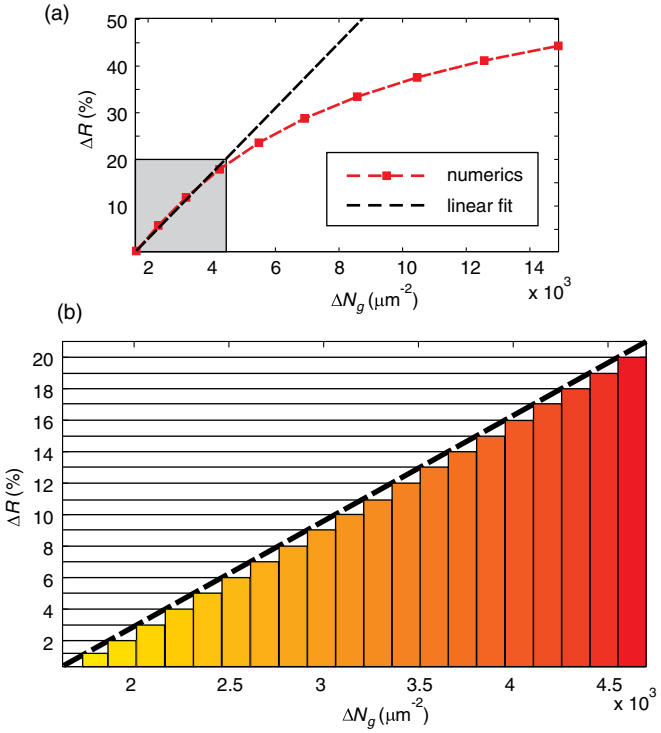

FIG. 7. Dynamic range of the sensor: change of the reflectance (in percent) as a function of the charge-carrier concentration in graphene for $E_{F,1} = 30$ meV, when ΔE_F goes up to 120 meV. ΔR is calculated numerically and by fitting with the linear curve with the slope $S_g = 6.7 \times 10^{-5}\ 1/\mu\text{m}^{-2}$. (b) Discrete steps during sensing, each step corresponds to the addition of 150 electrons or holes into graphene and an increase in the reflectance by 1%.

determined by the expression $n_d t_d = m\lambda_0/4$, where $m = 1, 3, 5, \ldots$. As shown in Fig. 5(d), the sensitivities at higher frequencies are only slightly decreased compared to the lowest resonance. Multiband operation is demonstrated in Fig. 8 showing the spectral dependence of the reflectance for $E_{F,1} = 30$ meV and for the graphene doped by $\Delta E_F = 3$ meV. Because of graphene doping, the reflectance is decreased by 1.15%, 1.1%, and 0.95% for the first ($f_{\text{res}} = 0.3$ THz), second ($f_{\text{res}} = 0.9$ THz), and third ($f_{\text{res}} = 1.5$ THz) resonance, respectively.

Sensitivity of the proposed graphene-covered terahertz resonators might be influenced by defects and inhomogeneities in graphene. They are especially pronounced in large graphene flakes required at terahertz frequencies. They mostly include electron-hole puddles, domain boundaries, and wrinkles, cracks, and multilayer islands, or they can be induced by nonuniform chemical doping from a medium to be sensed. As a result of these inhomogeneities, graphene Fermi energy and conductivity are nonuniform. In order to make possible numerical analysis, nonuniform Fermi energy is modeled as a one-dimensional periodic function with period P, two constant values within each period $E_1 = (1-\alpha)E_0$ and $E_2 = (1+\alpha)E_0$, where E_0 is

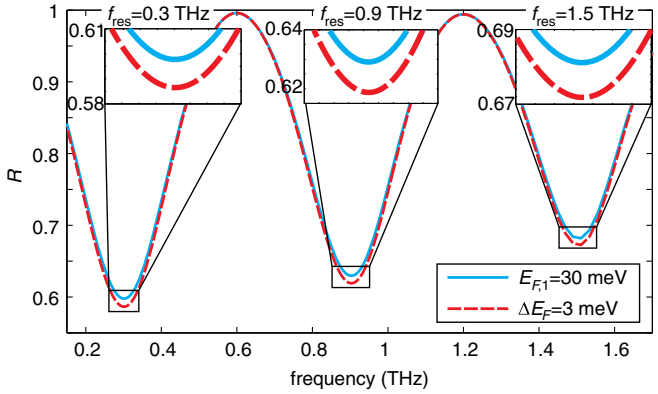

FIG. 8. Multiband operation of the sensor: reflectance as a function of frequency for $E_{F,1} = 30$ meV and $\Delta E_F = 3$ meV.

the Fermi energy of the homogeneous graphene, α is the inhomogeneity strength, whereas the filling fraction is kept fixed at 0.5, Fig. 9(a). In this case graphene consists of parallel and periodic ribbons with Fermi energies E_1 and E_2. Graphene nonuniformities are modeled in a similar way in Ref. [57]. Sensitivity S_g as a function of P, α, and for two polarizations is shown in Fig. 9(b). Sensitivity for homogeneous graphene is given for period $P \to \infty$. Apart from

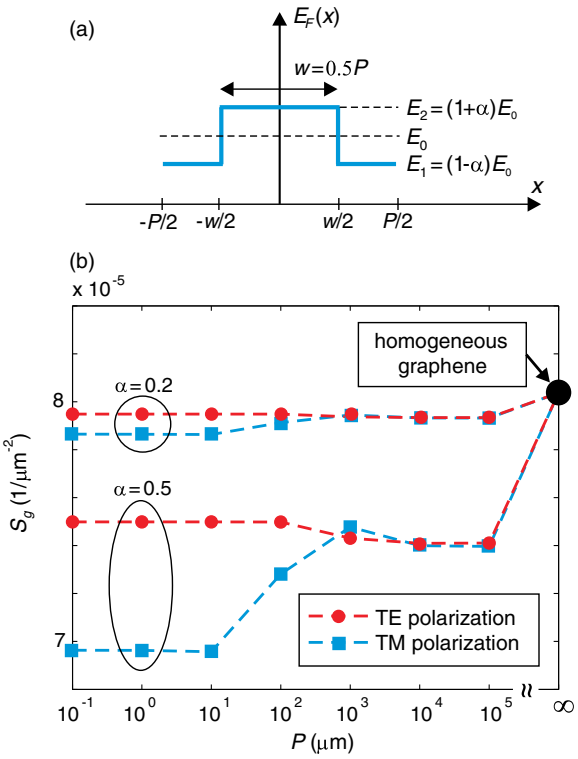

FIG. 9. (a) Inhomogeneous Fermi energy in graphene modeled as a periodic function with period P. (b) Sensitivity S_g as a function of inhomogeneity period P, strength α, and for two polarizations where in TM (TE) polarization the electric field of the incident field is polarized parallel (normal) to the direction of the periodicity [x direction in part (a)].

this point, the sensitivity slightly decreases, which is more pronounced for larger inhomogeneity strength α. For electron-hole puddles, typical variance of charge-density fluctuations is around 0.5×10^{11} cm^{-2} [58]. For considered $E_0 \approx 30$ meV, it follows that $E_1 \approx 20$ meV, $E_2 \approx 40$ meV, and the inhomogeneity strength $\alpha \approx 0.33$. As can be seen from Fig. 9(b), in this case S_g falls down by less than 10%.

VII. DISCUSSION

The considered graphene-covered terahertz resonators belong to the class of the affinity or nondirect sensors relying on the specific interaction between an analyte and the recognition element—graphene. The overall sensitivity $S = \alpha S_g$ depends on the factor α_g describing the efficiency of this interaction—the chemical doping. As mentioned above, α_g is equal to the ratio between the number of electrons or holes added to graphene and the number of adsorbed molecules causing this doping. In Ref. [4], α_g is given for the following molecules: H_2O, NH_3, CO, NO_2, and NO. The largest α_g around 0.1 is obtained for the NO_2 molecule. Taking into account the obtained resolution of around 150 electrons or holes per square micrometer, the proposed sensing structure can detect around 1500 molecules of NO_2 adsorbed per square micrometer. For other molecules, α_g is typically on the order of 10^{-2}, so the sensitivity is one order of magnitude smaller.

Standard affinity or nondirect chemical sensors require both the recognition element and the immobilization matrix necessary for the encapsulation of the recognition element [30]. On the other hand, graphene as a recognition element does not require any immobilization matrix, so the graphene-based chemical sensors can be made much simpler. Graphene can be used for sensing many different chemicals since it can be chemically doped by various gas molecules [2–4], biomolecules [10–13], metals, polymers, and organic molecules [5]. In addition, it can be easily functionalized, which further extends the range of molecules to be sensed. The adsorption of molecules on graphene is more efficient than on metallic substrates, which facilitates efficient chemical doping and sensing [14]. Beside the applications in the environment sensing, the proposed structure can be used for noninvasive and *in situ* monitoring of chemically doped and intercalated graphene.

While traditional optical sensors detect changes in the refractive index (either the real or imaginary part) of a surrounding medium, these changes are not considered in the presented analysis (air is taken as the surrounding medium with the constant refractive index equal to one). Therefore, proposed graphene-covered terahertz resonators enable the detection of tiny changes which cannot be detected with the traditional optical sensors.

In order to adjust the working point $E_{F,1}$ in graphene, it is necessary to apply bias voltage V_G between the metal electrode and graphene, as denoted in Fig. 3(a). This system can be considered as a capacitor with a capacitance per unit area $C_s = \varepsilon_0 n_d^2 / t_d$. Surface-charge density in graphene is then given by $N_g = C_s V_G / e$. Using the approximative formula for N_g from Eq. (5), V_g can be expressed as $V_g = e t_d E_F^2 / (\pi \varepsilon_0 \hbar^2 v_F^2 n_d^2)$. For the considered structure operating at 0.3 THz and $E_{F,1} = 30$ meV, V_g is around 850 V. Such high voltage is needed due to a low working frequency and required quarter-wavelength thickness of the dielectric spacer t_d (for f_0 around 1 THz, t_d is on the order of 100 μm). Very high-bias voltages are obviously not appropriate for practical purposes. In order to make this structure more realistic, instead of a homogeneous dielectric spacer in Fig. 3(a), a bilayer made from a low conductive silicon and silicon dioxide can be used [47]. The optical thickness of this bilayer should be still a quarter wavelength, but now the silicon can be used for graphene gating, while silicon dioxide can serve as a dielectric in this capacitor. The most important, thickness of the silicon dioxide, can now be adjusted at will, so V_g can be below 100 V.

For high Fermi energy $E_{F,1}$ around 0.5 eV, the proposed sensing structure operates as an almost perfect electromagnetic absorber since the reflectance tends to zero and absorbance is almost one (transmission is obviously zero due to the metallic bottom mirror). Then, any change from zero reflectance will give a very high relative change in the reflectance. This very efficient and simple method for sensing is proposed for electromagnetic absorbers based on plasmonic metamaterials [59]. However, due to the required very-high $E_{F,1}$, sensitivity S_g in this case would be very small as can be seen from Fig. 5(d). Still, we believe that critically coupled electromagnetic resonators covered with graphene and operating at a low Fermi energy would further enhance the sensitivity of graphene optical chemical sensors.

Graphene microstructures and nanostructures support localized surface-plasmon polaritons at terahertz and mid-infrared frequencies [60]. They alone act as electromagnetic resonators and can be utilized for refractive-index sensing [22,27,28]. However, it seems that they would hardly operate as chemical sensors since the localized surface-plasmon polaritons in graphene ribbon arrays are excited for high Fermi energies, 0.2–0.5 eV. Here, the sensitivity S_{E_F} given in Fig. 1(b) is very small, so the overall sensitivity would be low.

One of the most important advantages of optical detection over electrical detection in graphene-based chemical sensors is the possible selectivity in the sensing. Many molecules have active vibrational bands at terahertz frequencies [32,33]. The coupling of these molecular modes with the optical resonances of the proposed sensing structure would produce characteristic dips in the reflection spectra due to absorption. By detecting the position of these reflection dips, it would be possible to determine the type of

adsorbed molecules. The operating frequency of the sensor can be easily adjusted by the scaling thickness of the dielectric spacer t_d. This enables overlapping the sensor resonance with the frequency range where molecules to be sensed have active vibrational bands. In addition, the multiband operation of the sensors demonstrated in Fig. 8 enables the detection of different molecular modes simultaneously.

We believe there are two options for terahertz measurements. The first one is to use standard setups for terahertz spectroscopy. In this case, the whole reflectance spectra would be measured, while sensing would be done at a single frequency of the measured spectra corresponding to the resonance of the sensing structure. The second setup would include the terahertz quantum-cascade laser as a narrow-band source. In this case, the sensing structure would be designed with the resonance matching the excitation frequency of the laser. Sensing would then be done by the monitoring changes in the reflectance at this single frequency. However, in the second approach, the sensing cannot be selective.

Most of the absorption-based optical chemical sensors use optical fibers or planar waveguides and operate at visible frequencies. Here, we show that the sensitivity of graphene-based optical chemical sensors is maximized at terahertz frequencies. For this range, the most appropriate detection method is the terahertz spectroscopy. The sensitivity of the proposed graphene-based chemical sensors (on the order of 1 ppm) is similar to the sensitivity of standard terahertz gas sensors [61,62]. However, typical terahertz gas sensors require long cells (several meters) [56,61,63] in order to achieve a strong-enough absorption (the resolution limit is around 1% absorption). On the other hand, in graphene-based chemical sensors, absorption is not determined by the length of the cell since the absorption takes place within graphene. The ratio between the free-space wavelength (at 1 THz) and the thickness of the recognition element (graphene thickness of 0.34 nm) is extremely high—10^6. Therefore, graphene-based terahertz sensors can be made very compact, and this significantly advances terahertz sensing.

The sensitivity of graphene-covered optical waveguide sensors is on the order of 0.1 ppm [37,39]. This is one order of magnitude larger than the proposed graphene-covered terahertz resonators. This sensitivity is achieved using the interferometric interrogation in several-millimeters-long optical waveguides which already have high sensitivity on the order of 1 ppm. The working point of graphene (corresponding to Fermi energy $E_{F,1}$) is not controlled in these waveguide sensors, so the graphene optical conductivity should be constant at near-infrared frequencies, and it would be hardly influenced by chemical doping. Still, this sensing structure could be very useful for applications at the near-infrared and visible frequencies.

Sensing based on the intensity measurements at terahertz frequencies is considered instead of the wavelength interrogation at midinfrared frequencies due to better sensitivity, as discussed in detail in Sec. III. Still, sensing based on the wavelength interrogation at midinfrared frequencies could be possible due to the significant change of $\mathrm{Re}(\Delta\omega)$ according to Eq. (9). In Ref. [35], such a sensing method is considered for the midinfrared plasmonic nanoresonators coupled with chemically doped graphene for $E_{F,1}$ around 0.26 eV. The obtained resolution is estimated to be around $\Delta E_F \approx 25$ meV, which for the given $E_{F,1}$ corresponds to $\Delta N_g \approx 8.3 \times 10^3\ \mu\mathrm{m}^{-2}$. However, this is $50\times$ less compared to the proposed graphene-covered terahertz resonators with the resolution $\sigma \sim 150\ \mu\mathrm{m}^{-2}$. Better sensitivity at midinfrared frequencies could be achieved using electromagnetic resonators with very high-quality factors such as photonic-crystal cavities [50,51], so small spectral shifts of their sharp resonances due to chemical doping of graphene can be detected.

VIII. CONCLUSIONS

The graphene-covered terahertz resonator consisting of the metallic mirror with a quarter-wavelength-thick dielectric layer is proposed as a type of a chemical sensor with the optical detection. Graphene acts as a recognition element—it selectively interacts with adsorbed molecules, while the subsequent charge transfer leads to changes in the graphene conductivity. The terahertz resonator acts as a transducer—it provides electric-field enhancement within the graphene plane and transforms changes in the graphene conductivity into changes of the output reflectance. Graphene can be doped by various adsorbed molecules, so using graphene as a new type of recognition element in optical sensors enables detection of a wide range of chemicals. Their interaction with graphene takes place in a subwavelength layer, so the proposed sensing structure has a sensitivity not achievable with traditional optical sensors based on the refractive-index measurements.

ACKNOWLEDGMENTS

This work was supported by the Serbian Ministry of Education, Science and Technological Development under Project No. OI171005.

[1] K. S. Novoselov, A. K. Geim, S. V. Morozov, D. Jiang, Y. Zhang, S. V. Dubonos, I. V. Grigorieva, and A. A. Firsov, Electric field effect in atomically thin carbon films, Science **306**, 666 (2004).

[2] F. Schedin, A. K. Geim, S. V. Morozov, E. W. Hill, P. Blake, M. I. Katsnelson, and K. S. Novoselov, Detection of individual gas molecules adsorbed on graphene, Nat. Mater. **6**, 652 (2007).

[3] T. O. Wehling, K. S. Novoselov, S. V. Morozov, E. E. Vdovin, M. I. Katsnelson, A. K. Geim, and A. I. Lichtenstein, Molecular doping of graphene, Nano Lett. **8**, 173 (2008).
[4] O. Leenaerts, B. Partoens, and F. M. Peeters, Adsorption of H_2O, NH_3, CO, NO_2, and NO on graphene: A first-principles study, Phys. Rev. B **77**, 125416 (2008).
[5] H. Liu, Y. Liu, and D. Zhu, Chemical doping of graphene, J. Mater. Chem. **21**, 3335 (2011).
[6] Md. W. K. Nomani, R. Shishir, M. Qazi, D. Diwan, V. B. Shields, M. G. Spencer, G. S. Tompa, N. M. Sbrockey, and G. Koley, Highly sensitive and selective detection of NO_2 using epitaxial graphene on 6H-SiC, Sens. Actuators B **150**, 301 (2010).
[7] G. Ko, H.-Y. Kim, J. Ahn, Y.-M. Park, K.-Y. Lee, and J. Kim, Graphene-based nitrogen dioxide gas sensors, Curr. Appl. Phys. **10**, 1002 (2010).
[8] R. Pearce, T. Iakimov, M. Andersson, L. Hultman, A. Lloyd Spetz, and R. Yakimova, Epitaxially grown graphene based gas sensors for ultra sensitive NO_2 detection, Sens. Actuators B **155**, 451 (2011).
[9] S. Rumyantsev, G. Liu, M. S. Shur, R. A. Potyrailo, and A. A. Balandin, Selective gas sensing with a single pristine graphene transistor, Nano Lett. **12**, 2294 (2012).
[10] X. Dong, Y. Shi, W. Huang, P. Chen, and L.-J. Li, Electrical detection of DNA hybridization with single-base specificity using transistors based on CVD-grown graphene sheets, Adv. Mater. **22**, 1649 (2010).
[11] Y. Huang, X. Dong, Y. Shi, C. M. Li, L.-J. Li, and P. Chen, Nanoelectronic biosensors based on CVD grown graphene, Nanoscale **2**, 1485 (2010).
[12] P. K. Ang, M. Jaiswal, C. H. Y. X. Lim, Y. Wang, J. Sankaran, A. Li, C. T. Lim, T. Wohland, Ö. Barbaros, and K. P. Loh, A bioelectronic platform using a graphene-lipid bilayer interface, ACS Nano **4**, 7387 (2010).
[13] Y. Huang, X. Dong, Y. Liu, L.-J. Li, and P. Chen, Graphene-based biosensors for detection of bacteria and their metabolic activities, J. Mater. Chem. **21**, 12358 (2011).
[14] L. Wu, H. S. Chu, W. S. Koh, and E. P. Li, Highly sensitive graphene biosensors based on surface plasmon resonance, Opt. Express **18**, 14395 (2010).
[15] O. Salihoglu, S. Balci, and C. Kocabas, Plasmon-polaritons on graphene-metal surface and their use in biosensors, Appl. Phys. Lett. **100**, 213110 (2012).
[16] Q. Guo, H. Zhu, F. Liu, A. Y. Zhu, J. C. Reed, F. Yi, and E. Cubukcu, Silicon-on-glass graphene-functionalized leaky cavity mode nanophotonic biosensor, ACS Photonics **1**, 221 (2014).
[17] S. H. Choi, Y. L. Kim, and K. M. Byun, Graphene-on-silver substrates for sensitive surface plasmon resonance imaging biosensors, Opt. Express **19**, 458 (2011).
[18] J. C. Reed, H. Zhu, A. Y. Zhu, C. Li, and E. Cubukcu, Graphene-enabled silver nanoantenna sensors, Nano Lett. **12**, 4090 (2012).
[19] V. G. Kravets, R. Jalil, Y.-J. Kim, D. Ansell, D. E. Aznakayeva, B. Thackray, L. Britnell, B. D. Belle, F. Withers, I. P. Radko, Z. Han, S. I. Bozhevolnyi, K. S. Novoselov, A. K. Geim, and A. N. Grigorenko, Graphene-protected copper and silver plasmonics, Sci. Rep. **4**, 5517 (2014).
[20] C.-H. Lu, H.-H. Yang, C.-L. Zhu, X. Chen, and G.-N. Chen, A graphene platform for sensing biomolecules, Angew. Chem. **121**, 4879 (2009).
[21] L. Fei, Y. C. Jong, and S. S. Tae, Graphene oxide arrays for detecting specific DNA hybridization by fluorescence resonance energy transfer, Biosens. Bioelectron. **25**, 2361 (2010).
[22] B. Vasić, G. Isić, and R. Gajić, Localized surface plasmon resonances in graphene ribbon arrays for sensing of dielectric environment at infrared frequencies, J. Appl. Phys. **113**, 013110 (2013).
[23] Y. Zhao, X. Hu, G. Chen, X. Zhang, Z. Tan, J. Chen, R. S. Ruoff, Y. Zhu, and Y. Lu, Infrared biosensors based on graphene plasmonics: Modeling, Phys. Chem. Chem. Phys. **15**, 17118 (2013).
[24] J. Wu, C. Zhou, J. Yu, H. Cao, Shubin Li, and W. Jia, Design of infrared surface plasmon resonance sensors based on graphene ribbon arrays, Opt. Laser Technol. **59**, 99 (2014).
[25] K. Li, X. Ma, Z. Zhang, J. Song, Y. Xu, and G. Song, Sensitive refractive index sensing with tunable sensing range and good operation angle-polarization-tolerance using graphene concentric ring arrays, J. Phys. D **47**, 405101 (2014).
[26] R. Filter, M. Farhat, M. Steglich, R. Alaee, C. Rockstuhl, and F. Lederer, Tunable graphene antennas for selective enhancement of THz-emission, Opt. Express **21**, 3737 (2013).
[27] Y. Li, H. Yan, D. B. Farmer, X. Meng, W. Zhu, R. M. Osgood, T. F. Heinz, and P. Avouris, Graphene plasmon enhanced vibrational sensing of surface-adsorbed layers, Nano Lett. **14**, 1573 (2014).
[28] F. Liu and E. Cubukcu, Tunable omnidirectional strong light-matter interactions mediated by graphene surface plasmons, Phys. Rev. B **88**, 115439 (2013).
[29] F. Xing, Z.-B. Liu, Z.-C. Deng, X.-T. Kong, X.-Q. Yan, X.-D. Chen, Q. Ye, C.-P. Zhang, Y.-S. Chen, and J.-G. Tian, Sensitive real-time monitoring of refractive indexes using a novel graphene-based optical sensor, Sci. Rep. **2**, 908 (2012).
[30] C. McDonagh, C. S. Burke, and B. D. MacCraith, Optical chemical sensors, Chem. Rev. **108**, 400 (2008).
[31] J. Homola, Surface plasmon resonance sensors for detection of chemical and biological species, Chem. Rev. **108**, 462 (2008).
[32] A. I. McIntosh, B. Yang, S. M. Goldup, M. Watkinson, and R. S. Donnan, Terahertz spectroscopy: A powerful new tool for the chemical sciences?, Chem. Soc. Rev. **41**, 2072 (2012).
[33] M. Walther, B. M. Fischer, A. Ortner, A. Bitzer, A. Thoman, and H. Helm, Chemical sensing and imaging with pulsed terahertz radiation, Anal. Bioanal. Chem. **397**, 1009 (2010).
[34] F. J. Garcia de Abajo, Graphene nanophotonics, Science **339**, 917 (2013).
[35] Y. Xiao, Y. Francescato, V. Giannini, M. Rahmani, T. R. Roschuk, A. M. Gilbertson, Y. Sonnefraud, C. Mattevi, M. Hong, L. F. Cohen, and S. A. Maier, Probing the dielectric response of graphene via dual-band plasmonic nanoresonators, Phys. Chem. Chem. Phys. **15**, 5395 (2013).
[36] Y. Wu, B.-C. Yao, Y. Cheng, Y.-J. Rao, Y. Gong, W. Zhang, Z. Wang, and Y. Chen, Hybrid graphene-microfiber

waveguide for chemical gas sensing, IEEE J. Sel. Top. Quantum Electron. **20**, 49 (2014).

[37] B. Yao, Y. Wu, Y. Cheng, A. Zhang, Y. Gong, Y.-J. Rao, Z. Wang, and Y. Chen, All-optical Mach-Zehnder interferometric NH_3 gas sensor based on graphene/microfiber hybrid waveguide, Sens. Actuators B **194**, 142 (2014).

[38] B. C. Yao, Y. Wu, A. Q. Zhang, Y. J. Rao, Z. G. Wang, Y. Cheng, Y. Gong, W. L. Zhang, Y. F. Chen, and K. S. Chiang, Graphene enhanced evanescent field in microfiber multimode interferometer for highly sensitive gas sensing, Opt. Express **22**, 28154 (2014).

[39] Y. Wu, B. Yao, A. Zhang, Y. Rao, Z. Wang, Y. Cheng, Y. Gong, W. Zhang, Y. Chen, and K. S. Chiang, Graphene-coated microfiber Bragg grating for high-sensitivity gas sensing, Opt. Lett. **39**, 1235 (2014).

[40] T. Fang, A. Konar, H. Xing, and D. Jena, Carrier statistics and quantum capacitance of graphene sheets and ribbons, Appl. Phys. Lett. **91**, 092109 (2007).

[41] X. Sun, M. Lundstrom, and R. Kim, FD integral calculator, https://nanohub.org/resources/fdical.

[42] S. H. Mousavi, I. Kholmanov, K. B. Alici, D. Purtseladze, N. Arju, K. Tatar, D. Y. Fozdar, J. W. Suk, Y. Hao, A. B. Khanikaev, R. S. Ruoff, and G. Shvets, Inductive tuning of fano-resonant metasurfaces using plasmonic response of graphene in the mid-infrared, Nano Lett. **13**, 1111 (2013).

[43] G. W. Hanson, Dyadic Green's functions and guided surface waves for a surface conductivity model of graphene, J. Appl. Phys. **103**, 064302 (2008).

[44] G. Lovat, G. W. Hanson, R. Araneo, and P. Burghignoli, Semiclassical spatially dispersive intraband conductivity tensor and quantum capacitance of graphene, Phys. Rev. B **87**, 115429 (2013).

[45] Y. Yao, M. A. Kats, P. Genevet, N. Yu, Y. Song, J. Kong, and F. Capasso, Broad electrical tuning of graphene-loaded plasmonic antennas, Nano Lett. **13**, 1257 (2013).

[46] B. Vasić and R. Gajić, Graphene induced spectral tuning of metamaterial absorbers at mid-infrared frequencies, Appl. Phys. Lett. **103**, 261111 (2013).

[47] B. Sensale-Rodriguez, R. Yan, S. Rafique, M. Zhu, W. Li, X. Liang, D. Gundlach, V. Protasenko, M. M. Kelly, D. Jena, L. Liu, and H. G. Xing, Extraordinary control of terahertz beam reflectance in graphene electro-absorption modulators, Nano Lett. **12**, 4518 (2012).

[48] C.-C. Lee, S. Suzuki, W. Xie, and T. R. Schibli, Broadband graphene electro-optic modulators with sub-wavelength thickness, Opt. Express **20**, 5264 (2012).

[49] J. Kim, H. Son, D. J. Cho, B. Geng, W. Regan, S. Shi, K. Kim, A. Zettl, Y.-R. Shen, and F. Wang, Electrical control of optical plasmon resonance with graphene, Nano Lett. **12**, 5598 (2012).

[50] A. Majumdar, J. Kim, J. Vuckovic, and F. Wang, Electrical control of silicon photonic crystal cavity by graphene, Nano Lett. **13**, 515 (2013).

[51] X. Gan, R.-J. Shiue, Y. Gao, K. F. Mak, X. Yao, L. Li, A. Szep, D. Walker, J. Hone, T. F. Heinz, and D. Englund, High-contrast electrooptic modulation of a photonic crystal nanocavity by electrical gating of graphene, Nano Lett. **13**, 691 (2013).

[52] M. Engel, M. Steiner, A. Lombardo, A. C. Ferrari, H. v. Löhneysen, P. Avouris, and R. Krupke, Light-matter interaction in a microcavity-controlled graphene transistor, Nat. Commun. **3**, 906 (2012).

[53] M. Furchi, A. Urich, A. Pospischil, G. Lilley, K. Unterrainer, H. Detz, P. Klang, A. M. Andrews, W. Schrenk, G. Strasser, and T. Mueller, Microcavity-integrated graphene photodetector, Nano Lett. **12**, 2773 (2012).

[54] B. Vasić and R. Gajić, Tunable Fabry-Perot resonators with embedded graphene from terahertz to near-infrared frequencies, Opt. Lett. **39**, 6253 (2014).

[55] J. P. Hugonin and P. Lalanne, *RETICOLO Code for Grating Analysis* (Institute d'Optique, Palaiseau, France, 2005).

[56] J. S. Melinger, Y. Yang, M. Mandehgar, and D. Grischkowsky, THz detection of small molecule vapors in the atmospheric transmission windows, Opt. Express **20**, 6788 (2012).

[57] J. L. Garcia-Pomar, A. Y. Nikitin, and L. Martin-Moreno, Scattering of graphene plasmons by defects in the graphene sheet, ACS Nano **7**, 4988 (2013).

[58] J. Martin, N. Akerman, G. Ulbricht, T. Lohmann, J. H. Smet, K. von Klitzing, and A. Yacoby, Observation of electron-hole puddles in graphene using a scanning single-electron transistor, Nat. Phys. **4**, 144 (2008).

[59] N. Liu, M. Mesch, T. Weiss, M. Hentschel, and H. Giessen, Infrared perfect absorber and its application as plasmonic sensor, Nano Lett. **10**, 2342 (2010).

[60] L. Ju, B. Geng, J. Horng, C. Girit, M. Martin, Z. Hao, H. A. Bechtel, X. Liang, A. Zettl, Y. R. Shen, and F. Wang, Graphene plasmonics for tunable terahertz metamaterials, Nat. Nanotechnol. **6**, 630 (2011).

[61] E. Gerecht, K. O. Douglass, and D. F. Plusquellic, Chirped-pulse terahertz spectroscopy for broadband trace gas sensing, Opt. Express **19**, 8973 (2011).

[62] B. You, C.-H. Ho, W.-J. Zheng, and J.-Y. Lu, Terahertz volatile gas sensing by using polymer microporous membranes, Opt. Express **23**, 2048 (2015).

[63] A. M. Fosnight, B. L. Moran, and I. R. Medvedev, Chemical analysis of exhaled human breath using a terahertz spectroscopic approach, Appl. Phys. Lett. **103**, 133703 (2013).